SIAM J. APPL. MATH.
Vol. 62, No. 6, pp. 2045–2063


# THE THICKNESS OF A MARANGONI-DRIVEN THIN LIQUID FILM EMERGING FROM A MENISCUS*

ANDREAS MÜNCH†

**Abstract.** In this paper, we revisit experiments in which a thin liquid film forms at the tip of a capillary meniscus due to the presence of a thermally induced Marangoni shear stress. Starting from basic fluid mechanical equations, we devise a model for which numerical solutions show that it is able to accurately predict the thickness of the film, in contrast to earlier theories [Fanton, Cazabat, and Quéré, *Langmuir*, 12 (1996), pp. 5875–5880], where discrepancies with the experimental data of up to 20% were observed. We then find that only a few terms of our model yield a significant contribution to the film thickness. For the resulting reduced model, we derive an approximate, matched asymptotic solution, valid for small capillary numbers, which, to leading order, recovers the result of the older theory. Extending the calculation to the next order yields a correction that substantially improves the accuracy.

**Key words.** lubrication theory, matched asymptotics, Marangoni shear stress, surface tension, Landau–Levich drag-out problem, logarithmic switchback terms

**AMS subject classifications.** 34B60, 34E05, 34E10, 34E15, 35Q30, 76D07, 76D27, 76D45, 76M45, 76A20, 76D08

**PII.** S0036139900382693

## 1. Introduction.

In recent years, various aspects of the formation and behavior of thin liquid films that climb out of a reservoir along an inclined wafer under the action of a thermally induced Marangoni shear stress have been intensively investigated, e.g., [5, 4, 6, 9, 10, 2]. The basic setup, introduced in the first reference, is shown in Figure 1.1. A silicon wafer, tilted at an angle $\alpha$ from the vertical position, is subject to a temperature gradient between two heaters that maintain a temperature of $T_+$ at its lower end and of $T_- < T_+$ at its upper end. The lower end of the wafer is submerged in a reservoir of silicon oil. At the beginning of the experiment the level of the liquid in the reservoir is kept below the region where the temperature gradient sets in. The fluid therefore achieves a thermal and hydrostatic equilibrium, with a meniscus that extends a certain distance up the wafer.

Then, the liquid of the reservoir is raised, by slowly adding liquid from an external reservoir (not shown in the figure), until the meniscus just reaches into the thermal gradient region. As a result, the liquid in the upper part of the meniscus experiences a thermal gradient, which leads to a gradient in the temperature dependent surface tension coefficient, so that the surface tension decreases in the upwards direction. Consequently, a Marangoni shear stress sets in at the liquid/air interface, which pulls a thin film of liquid out of the reservoir, up along the wafer.

Once the contact-line has moved sufficiently far from the reservoir's surface, the meniscus region and the adjacent film become stationary, and the latter becomes flat. Let $h_\infty$ denote the constant film thickness. Towards the rising contact-line, the film evolves into either a single traveling wave or a double wave structure. Various aspects of these structures and the transitions between them have been studied intensively

*Received by the editors December 19, 2000; accepted for publication (in revised form) December 17, 2001; published electronically July 3, 2002. This research was supported by a habilitation grant from the German Science Foundation (DFG), grant number MU 1626/1-1.

http://www.siam.org/journals/siap/62-6/38269.html

†Zentrum Mathematik (H4), TU München, 82090 Munich, Germany (amue@appl-math.tu-muenchen.de).

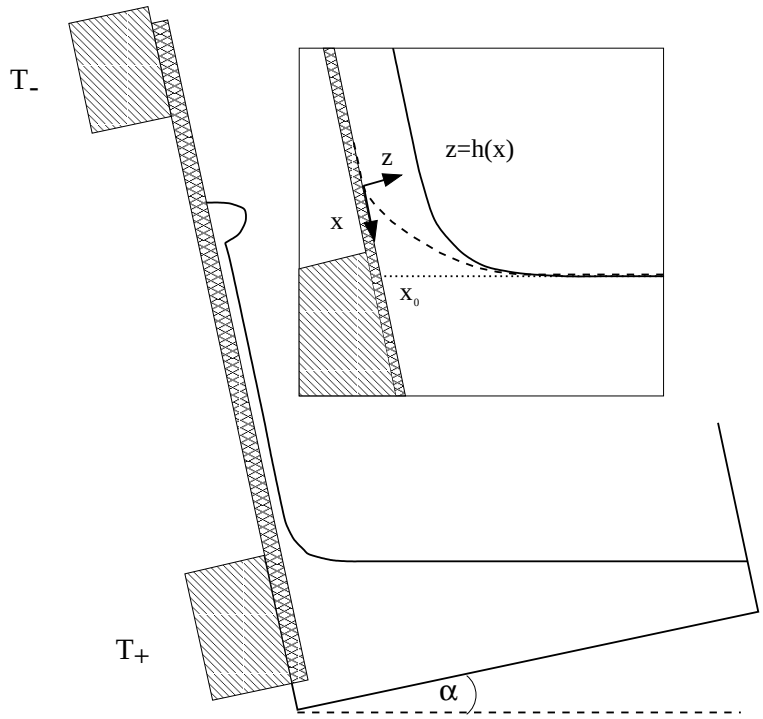


FIG. 1.1. *Sketch of the experimental setup. The dashed and dotted lines in the inset indicate, respectively, the position of the static meniscus that is achieved as equilibrium position in the absence of thermal gradients and the level of the undisturbed surface of the liquid in the reservoir.*

in experimental and theoretical papers [14, 9, 10, 2, 3, 18, 17, 19]. It was found that the film thickness plays an important role in determining the outcome, i.e., which of the different wave structures evolve. The film thickness was usually treated as an independent parameter in the theoretical investigations, but, for the experimental setup discussed here and in most of the above references, $h_\infty$ is really determined by the force balance in the meniscus. Our chief interest in this paper will be to determine $h_\infty$ for given inclination angle, thermal gradient, and fluid properties.

The problem is reminiscent of the situation investigated in a classical paper by Landau and Levich [12], where a flat plate is pulled out of a pool of liquid. Using ideas from singular perturbation theory, the authors show that $h_\infty$ is determined by a balance of gravitational, capillary, and viscous forces, and they derive an asymptotic formula for $h_\infty$ in terms of the fluid properties and the withdrawal velocity. This approach was adapted by [4, 6] to the situation with a thermal Marangoni stress as driving force, and compared with their experiments. The experimental results for $h_\infty$ indeed agree with the scaling predicted by the asymptotic formula, but in the second reference, the authors observe a systematic discrepancy between the predicted and the experimentally obtained values of about 20%. They attribute this to a shortcoming in the asymptotic matching procedure used in the derivation. In our paper, we will reconsider the theory, with the aim of improving the theoretical prediction, and we will explain the discrepancy that was observed previously.

In section 2, we formulate a stationary model for the meniscus region, starting from the basic fluid mechanical equations, and solve it numerically, in section 3. We

find that the results for our model agree nicely with the experimental data from [6]; i.e., they remove the discrepancy observed for the comparison with the earlier prediction. Taking up ideas by Wilson [21] for the drag-out problem, we find we can simplify the model equations to a single third order ODE, with only little change in the computed film thickness. In section 4, our matched asymptotic solution then yields, to leading order, the formula obtained by [4, 6]. We show that their experiments lie in the range where higher order approximations are indeed needed. We find that to be able to match to next order, the effect of the flow-field in the outer region has to be taken into account. As a consequence, the correction for the film thickness reduces the discrepancy substantially.

**2. Formulation.** We introduce a system of coordinates as indicated in the inset of Figure 1.1, with the positive $x$-axis pointing along the wafer towards the reservoir, and the $z$-axis normal to it. The origin is placed at the tip of the static meniscus, which is located at a distance $x_0$ along the $x$-axis, with respect to the surface of the undisturbed reservoir. The value of $x_0$ depends solely on the inclination angle $\alpha$ and on the capillary length $L = (\sigma/(\rho g))^{1/2}$, where $g$, $\rho$, and $\sigma$ denote the gravitational acceleration, the liquid density, and the surface tension coefficient of the liquid/air interface. For the derivation of an explicit expression for $x_0$, we refer to the appendix.

In the bulk, the two velocity components $v$ and $w$ in the $x$ and $z$ directions, the pressure field $p$, and the temperature $T$ are governed by the Stokes equation coupled to the continuity and energy equation:

$$\begin{aligned} -p_x + \mu(u_{xx} + u_{zz}) + \rho g \cos\alpha &= 0, \\ -p_z + \mu(w_{xx} + w_{zz}) - \rho g \sin\alpha &= 0, \\ u_x + w_z &= 0, \\ k_{\mathrm{th}}(T_{xx} + T_{zz}) - \rho c(uT_x + wT_z) &= 0. \end{aligned}$$

Here, $\mu$, $c$, and $k_{\mathrm{th}}$ denote the viscosity, specific heat, and thermal conductivity of the silicon oil, respectively. Neglecting inertia is reasonable in view of the very slow spreading of the liquid film, which rises at about 1 mm per minute. Furthermore, the Reynolds number strongly depends on the viscosity, so that any effect of inertia on the film thickness $h_\infty$ would be expected to vary significantly for fluids with different viscosity. The experimental studies [6] emphasize, however, that $h_\infty$ did not change significantly, even though the authors used several PDMS oils with viscosities differing by more than one order of magnitude but otherwise with similar material properties.

At the surface of the wafer, we have the usual no-slip and impermeability conditions,

$$u = w = 0 \qquad \text{at} \quad z = 0.$$

At the liquid/air interface, i.e., at $z = h(x)$, we have the kinematic condition and the two equations for the tangential and normal stresses:

$$w - uh_x = 0,$$

$$2h_x(w_z - u_x) + (1 - h_x^2)(u_z + w_x) = -\frac{\sigma_T}{\mu}(T_x + T_z h_x)(1 + h_x^2)^{1/2}, \tag{2.1}$$

$$-p + 2\mu\frac{u_x h_x^2 + w_z - h_x(u_z + w_x)}{1 + h_x^2} = \frac{\sigma h_{xx}}{(1 + h_x^2)^{3/2}}. \tag{2.2}$$

The right-hand side of (2.1) represents the Marangoni shear stress, which arises at the surface of the liquid due to the variation of the surface tension coefficient $\sigma$ along

the surface. This in turn results from the temperature dependence of $\sigma$, which we assume here to be approximately linear, $\sigma = \sigma|_{T_+} - \sigma_T(T - T_+)$. The constant $\sigma_T$ is positive for most liquids, so that, with the temperature decreasing in the direction up the wafer, the Marangoni stress drives the upward motion of the liquid in the film. Nevertheless, the total change experienced by $\sigma$ over the meniscus region is small, so that in the normal stress condition (2.2) we can use a Boussinesque-type approximation and keep $\sigma \equiv \sigma|_{T_+}$ constant. Similarly, all other material coefficients $\mu$, $\rho$, etc., are taken to be constant and are set equal to their values at $T = T_+$.

For the temperature field, we assume that the heat transfer into the surrounding air is negligible,

$$T_z - h_x T_x = 0.$$

The boundary condition for $T$ at the wafer ($z = 0$) requires some discussion. Due to the good thermal conductive properties of the silicon wafer, and the negligible heat loss through the thin film, the temperature gradient at the wafer is constant and equal to $T_+ - T_-$ divided by the distance $d_h$ of the heaters, except near the heaters themselves, where $T$ approaches a constant temperature (either $T_-$ or $T_+$). In [5], the authors state that at the beginning of the experiment the level of fluid is slowly raised to where the meniscus *just* reaches into the thermal region. Therefore, they conclude that the meniscus is located in a region of the wafer where the temperature gradient has not quite reached its maximal value $(T_+ - T_-)/d_h$.

Direct measurements of the temperature profile in the meniscus zone were not supplied in the experimental observations [6]. Instead, the authors adjust the temperature gradient to a value smaller than $(T_+ - T_-)/d_h$ so that the shape of the computed meniscus agrees with the shape of the measured meniscus. For these computations, they use a lubrication model for the front part of the meniscus. This suggests that, to compare our results with the experimental data in [6], we use the following temperature profile at $z = 0$,

$$T = T_+ + \gamma\,\Omega(x), \qquad \text{with} \quad \Omega(x) = \begin{cases} x - \omega x_0 & \text{for} \quad x \le \omega x_0, \\ 0 & \text{otherwise,} \end{cases} \tag{2.3}$$

where $\gamma$ denotes their adjusted value for the temperature gradient. The gradient is cut-off at $\omega x_0 > 0$, which takes into account that beyond a certain point $\omega x_0$, the wafer temperature is constant and equal to $T_+$. As we mentioned before, the references indicate that only the front part of the meniscus is placed in the temperature gradient zone. We therefore restrict $\omega$ to $\omega < 1$, so that (2.3) provides a cut-off above the level of the reservoir.

Once the contact line region has risen far enough, the film can be considered to have a constant thickness at some distance from the meniscus,

$$\lim_{x\to-\infty} h = h_\infty, \quad \lim_{x\to-\infty} h_x = 0, \quad \lim_{x\to-\infty} h_{xx} = 0. \tag{2.4}$$

In the other direction, the meniscus flattens out onto the surface of the undisturbed reservoir,

$$\lim_{x\to\infty} (h - (x - x_0)\cot\alpha) = 0, \quad \lim_{x\to\infty} h_{xx} = 0. \tag{2.5}$$

In this form, this boundary condition is only applicable for $\alpha \neq 0$, otherwise, the slope of the reservoir's surface becomes infinite. As a simple remedy, we could replace (2.5)

with the condition that $h$ becomes infinite for some finite $x$ and that simultaneously, the curvature $h_{xx}(1+h_x^2)^{-3/2}$ tends to zero. We avoid the technical complication of discussing various cases (positive, zero, and even negative $\alpha$) by requiring $\alpha > 0$. For a treatment of the equivalent cases within the context of the drag-out problem, see [21].

The corresponding boundary conditions for $u$, $w$, and $T$ are obtained from an open channel flow with a constant shear stress at the surface,

$$\lim_{x\to-\infty} u = -\frac{\rho g\cos\alpha}{\mu}\left(\frac{z^2}{2} - zh_\infty\right) - \frac{\sigma_T\gamma}{\mu}z, \quad \lim_{x\to-\infty} w = 0, \quad \lim_{x\to-\infty} T_x = \gamma. \tag{2.6}$$

Towards the reservoir, we require

$$\lim_{x\to\infty} u = 0, \quad \lim_{x\to\infty} w = 0, \quad \lim_{x\to\infty} T_x = 0. \tag{2.7}$$

The situation we are considering is essentially that of a nearly static meniscus which is only slightly perturbed by a creeping flow of liquid into a thin film at its tip. It is therefore reasonable to choose a scaling where hydrostatic and capillary forces balance. Thus we use the capillary length $L$ as a scale for $x$ and $z$, and $(\sigma\rho g)^{1/2}$ for $p$. Since $\Omega \sim x$ for $x \le \omega x_0$, we scale $\Omega$ and $T - T_+$ with $L$ and $\gamma L$, respectively. The velocity scales for $u$ and $w$ are obtained by balancing the terms in the continuity equation and the tangential stress condition (2.1) and are found to be $U = (\sigma_T\gamma/\mu)L$ for both velocity components.

Introducing these scalings, we obtain the dimensionless equations

$$-p_x + 2\delta(u_{xx} + u_{zz}) + \cos\alpha = 0, \tag{2.8}$$

$$-p_z + 2\delta(w_{xx} + w_{zz}) - \sin\alpha = 0, \tag{2.9}$$

$$u_x + w_z = 0, \tag{2.10}$$

$$T_{xx} + T_{zz} - \mathrm{Pe}\,(uT_x + wT_z) = 0 \tag{2.11}$$

in the bulk,

$$u = w = 0 \qquad \text{and} \qquad T = \Omega(x) \tag{2.12}$$

at $z = 0$, and

$$w - uh_x = 0, \tag{2.13}$$

$$2h_x(w_z - u_x) + (1-h_x^2)(u_z + w_x) = -(T_x + T_z h_x)(1+h_x^2)^{1/2}, \tag{2.14}$$

$$-p + 4\delta\frac{u_x h_x^2 + w_z - h_x(u_z + w_x)}{1+h_x^2} = \frac{h_{xx}}{(1+h_x^2)^{3/2}}, \tag{2.15}$$

$$T_z - h_x T_x = 0 \tag{2.16}$$

at $z = h(x)$. The conditions at (2.4), (2.5), and (2.7) remain the same in dimensionless variables, so we do not repeat them here; for (2.6), we get

$$\lim_{x\to-\infty} u = -\frac{\cos\alpha}{2\delta}\left(\frac{z^2}{2} - zh_\infty\right) - z, \quad \lim_{x\to-\infty} w = 0, \quad \lim_{x\to-\infty} T_x = 1. \tag{2.17}$$

Two dimensionless parameters other than $\alpha$ appear in these equations, the capillary number

$$\delta^2 = \frac{\mu U}{\sigma} = \frac{\sigma_T^2\gamma^2}{4\sigma\rho g} \ll 1,$$

which measures the relative importance of viscous to the mean capillary forces, and the Péclet number

$$\mathrm{Pe} = \frac{\rho c U L}{k_{\mathrm{th}}} = \frac{c}{k_{\mathrm{th}}} \frac{\sigma_T \gamma \, \sigma}{\mu g}.$$

The Péclet number measures the relative importance of the two mechanisms of heat distribution, namely convection and diffusion. For the fluids and temperature gradients $\gamma$ used in the experiments discussed here, we found Pe to be quite large, up to about 200. For the numerical computations, the Péclet number was chosen from a range of values near this upper bound.

**3. Numerical results and derivation of an approximate model.** We begin by solving the model equations (2.3)–(2.5), (2.7)–(2.17) numerically. For this purpose, we first rewrite the equation using a stream-function formulation $u = \psi_z$, $w = -\psi_x$. This yields

$$\psi_{xxxx} + 2\psi_{xxzz} + \psi_{zzzz} = 0, \qquad T_{xx} + T_{zz} - \mathrm{Pe}(\psi_z T_x - \psi_x T_z) = 0 \tag{3.1}$$

in the bulk,

$$\psi = \psi_z = 0 \qquad \text{and} \qquad T = \Omega(x) \tag{3.2}$$

at $z = 0$, and

$$\frac{d}{dx}\psi = 0, \tag{3.3}$$

$$-4h_x\psi_{xz} + (1 - h_x^2)(\psi_{zz} - \psi_{xx}) = -(T_x + T_z h_x)(1 + h_x^2)^{1/2}, \tag{3.4}$$

$$\frac{d}{dx}\left(\frac{h_{xx}}{(1 + h_x^2)^{3/2}}\right) = 2\delta R - \cos\alpha + h_x \sin\alpha, \tag{3.5}$$

$$T_z - h_x T_x = 0, \tag{3.6}$$

where

$$\begin{aligned} R = {} & -\psi_{xxz} - \psi_{zzz} + (\psi_{xxx} + \psi_{xzz})h_x \\ & -2\frac{d}{dx}\left(\frac{(1 - h_x^2)\psi_{zx} + h_x(\psi_{zz} - \psi_{xx})}{1 + h_x^2}\right) \end{aligned} \tag{3.7}$$

at the surface $z = h(x)$.

At $x \to -\infty$ we impose boundary conditions for a flat film,

$$\lim_{x \to -\infty} h_{xx} = 0, \tag{3.8}$$

and the corresponding flow (equivalent to (2.17)),

$$\lim_{x \to -\infty} \psi = -\frac{\cos\alpha}{2\delta}\left(\frac{z^3}{6} - \frac{z^2}{2}h_\infty\right) - \frac{z^2}{2}, \quad \lim_{x \to -\infty} \psi_x = 0, \quad \lim_{x \to -\infty} T_x = 1, \tag{3.9}$$

and at $\infty$, the conditions for a flat reservoir,

$$\lim_{x \to \infty} (h_x - \cot\alpha) = 0, \quad \lim_{x \to \infty} h_{xx} = 0, \tag{3.10}$$

as well as

$$\lim_{x\to\infty} \psi_x = 0, \quad \lim_{x\to\infty} \psi_{xx} = 0, \quad \text{and} \quad \lim_{x\to\infty} T_x = 0. \tag{3.11}$$

In order to get a fixed boundary problem on a rectangular domain, which is more amenable to finite difference discretization, we first truncate the domain in the $x$ direction at $x_b < 0$ and $x_e > 0$ and impose the boundary conditions (3.8)–(3.11) at $x_b$, $x_e$ instead of at $\pm\infty$. For the practical implementation, it is of course important to make a reasonable choice for the size of the domain, i.e., for $x_b$ and $x_e$; a typical choice was $x_b = -5$ and $x_e = 11$. We remark that in the actual code, we implement the condition for the stream-function at the right end of the computational domain using derivatives with respect to the fixed-domain variables $(x, \zeta)$.

The truncated problem is then mapped to the domain $[x_b, x_e] \times [0, 1]$ via the substitution $\zeta = z/h(x)$. Since the resulting equations are rather bulky, in particular, where high order derivatives in $x$ are transformed, we do not spell them out here.

The problem thus obtained can then be discretized using finite differences in both the $x$ and $z$ directions. The resulting nonlinear algebraic problem (which we refer to by the numbers of their untransformed, continuous counterparts, with a subscript $d$ attached for distinction) is solved iteratively. We first keep the $h$ fixed (we do not distinguish between the vector of discrete values on the finite difference grid and the function it represents) and solve $(3.1)_d$–$(3.4)_d$, $(3.6)_d$, the corresponding boundary conditions at $x_b$ and $x_e$, but we drop the normal stress condition $(3.5)_d$, $(3.7)_d$. This represents a coupled algebraic problem for the discretized stream-function $\psi$ and temperature field $T$, which is nonlinear due only to the convective term in the temperature equation. We deal with this subproblem in an inner iteration loop by alternately solving for $\psi$ and $T$.

The linear algebraic systems are solved through standard direct band solvers [1], which is quite effective because we found that we needed only few grid points in the $z$ direction, much less than in the $x$-coordinate. By counting the discretization nodes in the order $z$-by-$x$ direction, one therefore arrives at linear algebraic systems with a quite densely banded matrix. Since the discretization of high order differential equations in combination with the separation of scales—an order one meniscus region is connected with a thin film that is as thin as 0.001—tends to lead to ill-conditioned linear problems, we found it was useful for an accurate and stable code to perform the calculations in quadruple precision.

We checked the numerical solution for the stream-function by verifying that the flow was a lubrication flow at the left end of the computational domain (near $x_b$) and that at the right end (towards $x_e$) it was a superposition of Moffatt's solution for the far-field behavior of flow in a wedge [15] and an additional contribution that reflects the mass loss through the thin film (see also [8]).

Once we have obtained the solution for the stream-function, we can evaluate the normal stress condition $(3.5)_d$, $(3.7)_d$. Each choice of $h$ will yield, through the above procedure, a residual vector for $(3.5)_d$, i.e., a vector of values for the difference of left- and right-hand side, which is usually nonzero, unless $h$ is a (discrete) solution. We can thus find a solution by treating $(3.5)_d$, $(3.7)_d$ as a nonlinear system of equations for $h$, which we can deal with in an outer iteration loop using Newton's method.

Since $(3.7)_d$ represents the discretization of a nonlocal operator of $h$, due to its dependence on the full flow-field, the resulting Jacobian is dense; we can replace it by an approximate Jacobian that is essentially banded if we use a lubrication approximation of the full stream-function/temperature field. This approximation is

used only for the computation of the Jacobian; of course, the residual is still evaluated using the solution for $\psi$ and $T$ for the full problem.

Also, the formulation (3.1)–(3.11) on which the discrete problem is based does not fix the location of $h$ with respect to the origin. Hence the problem permits a whole family of solutions, which correspond to different positions of the surface of the reservoir; i.e., each member of the family asymptotes, for large positive $x$ to a different line, have the same slope but a different point of intersection with the $x$-axis. The model formulation in the previous section, however, specifies via (2.5) that the line to which the solution asymptotes has to intersect the $x$-axis at $x_0$. Respecting this requirement is relevant since the boundary value problem is nonautonomous due to the heating profile $\Omega(x)$. A corresponding condition for the truncated problem is, for example, that

$$h(x_e) = (x_e - x_0)\cot\alpha \tag{3.12}$$

be satisfied. Enforcing (3.12) directly as a boundary condition at $x_e$ seems to be a good idea at first, but in practice, the Newton iterations did not converge reliably. We take up an idea that has proven to be useful when computing invariant manifolds connecting fixed points (see, for example, [7] and references therein) and formulate a phase condition for $h$. We start with the present formulation $(3.1)_d$–$(3.11)_d$, linearize it to obtain a linear algebraic problem for the Newton corrections, and replace one of the linearized equations by the phase condition. The phase condition minimizes the amount by which the Newton correction "shifts" the solution with respect to a reference profile, typically the initial profile used to start the Newton iterations.

The phase condition can be more easily described for the continuous profile on an infinite domain. Let $h_r$ denote the reference profile, which we assume fulfills the far-field conditions (2.4) and (2.5), and let $h^{(i)}$ be a sequence of profiles that approximate the continuous profile $h(x)$, with $h^{(0)} := h_r$. The family of exact continuous profiles is denoted by $h(x;\lambda)$. We assume the parameterization $\lambda$ is chosen so that $\lambda = 0$ selects the member which is "closest" to the reference profile, in the sense that it satisfies

$$\int_{-\infty}^{\infty} \left| \left(\frac{1}{h(x;\lambda)}\right)_x - \left(\frac{1}{h_r(x)}\right)_x \right|^2 dx \stackrel{!}{=} \min.$$

Here we compare the derivatives of the inverse of the profiles instead of comparing the profiles themselves because only the former functions decay to zero at $\pm\infty$. A necessary condition for a minimum at $\lambda = 0$ is

$$\int_{-\infty}^{\infty} \left( \left(\frac{1}{h(x;\lambda)}\right)_x - \left(\frac{1}{h_r(x)}\right)_x \right) \frac{d}{d\lambda} \left(\frac{1}{h(x;\lambda)}\right)_x dx = 0 \qquad \text{at} \quad \lambda = 0.$$

For the case where the heater profile is trivial ($\Omega' \equiv 1$), the family of solutions is obtained by shifting along the $x$-axis, so that $d/d\lambda\,(1/h(x;\lambda))_x$ for $\lambda = 0$ is equal to $(1/h(x;0))_{xx}$. This is approximately true only if $\Omega$ is chosen as in (2.3) with finite $\omega$; the profiles, and the thickness $h_\infty$, change as they are shifted. But nevertheless we found that replacing the derivative in $\lambda$ by $(1/h(x;0))_{xx}$ results in a phase condition that works in practice. Using that $\int_{-\infty}^{\infty} (1/h)_x (1/h)_{xx}\, dx = 0$, we obtain the condition

$$\int_{-\infty}^{\infty} \left(\frac{1}{h_r}\right)_x \left(\frac{1}{h}\right)_{xx} dx = 0.$$

This condition is certainly satisfied by the initial profile $h^{(0)} = h_r$ and by virtue of the conditions (2.4) and (2.5). It is also fulfilled by all subsequent iterates $h^{(i)}$, if

$$\int_{-\infty}^{\infty} \left( \frac{1}{h^{(i+1)}} - \frac{1}{h^{(i)}} \right) \left( \frac{1}{h_r} \right)_{xxx} dx = 0 \tag{3.13}$$

holds for all $i \geq 0$; note that we have integrated by parts. For the practical implementation of the algorithm, we replace (3.13) by the following linearized condition for the correction $\Delta h := h^{(i+1)} - h^{(i)}$:

$$\int_{-\infty}^{\infty} \frac{\Delta h}{\left(h^{(i)}\right)^2} \left( \frac{1}{h_r} \right)_{xxx} dx = 0. \tag{3.14}$$

From this, the corresponding conditions for the Newton corrections of the discrete profiles are obtained in a straightforward way by replacing the integral by a discrete inner product and the derivatives by finite differences.

We found that, in practice, the resulting Newton scheme not only converged, that is, the residuals quickly dropped below a prescribed threshold, but also produced solutions which fulfilled (3.12) quite well, if the initial profile was close to a solution. Where the converged result was not satisfactory, it was shifted so that it satisfied (3.12), and then the Newton iterations were restarted using the shifted $h$ as the new initial/reference profile.

Finally, we remark that we found it was advantageous to interlace the inner and outer iterations, i.e., update the free surface before the inner iterations had produced accurate results for $T$ and the stream-function.

We compare our numerical results for different inclination angles and for different choices of $\omega$ with experiments in [6] and with the asymptotic prediction for $h_\infty$ given in that reference. Their formula reads in our dimensionless variables

$$h_\infty = 13.7\Delta, \qquad \Delta := \frac{\delta^2}{2} \left( \frac{2}{1 - \sin\alpha} \right)^{3/2}. \tag{3.15}$$

This prediction appears as a straight line in Figure 3.1, where we plot $h_\infty$ versus $\Delta$. As found by [6], the experimental data points indeed seem to gather around a single straight line, even if $\alpha$ is varied, but its slope is about 11, i.e., 20% less than in (3.15). In fact, the prediction overestimates the film thickness for every single data point included in Figure 9 of that reference. This is particularly surprising since the temperature gradient used in [6] for the evaluation of the asymptotic formula—which is also the one we based our $\delta$ on—is the adjusted value. Recall that the adjusted value is the one for which the shape of the meniscus near the flat film computed numerically by [6] via a simplified model agreed best with the measured profile. Therefore, we would expect good agreement between measured thickness and predictions from numerical solutions for the meniscus shape, as well as for sufficiently accurate asymptotic approximations. However, for the asymptotic formula (3.15), this is not the case; its prediction differs significantly from the experimental results.

In contrast, our numerical results, shown in Figure 3.1 for different inclination angles and different $\omega$, agree quite well with the experimental line $h_\infty = 11\Delta$. This indicates that the higher order effects which have been neglected in the derivation of (3.15) are responsible for the discrepancy. Further support comes from the observation that, in general, agreement with the experimental and the numerical data is better for small values of $\delta$, i.e., of $\Delta$.

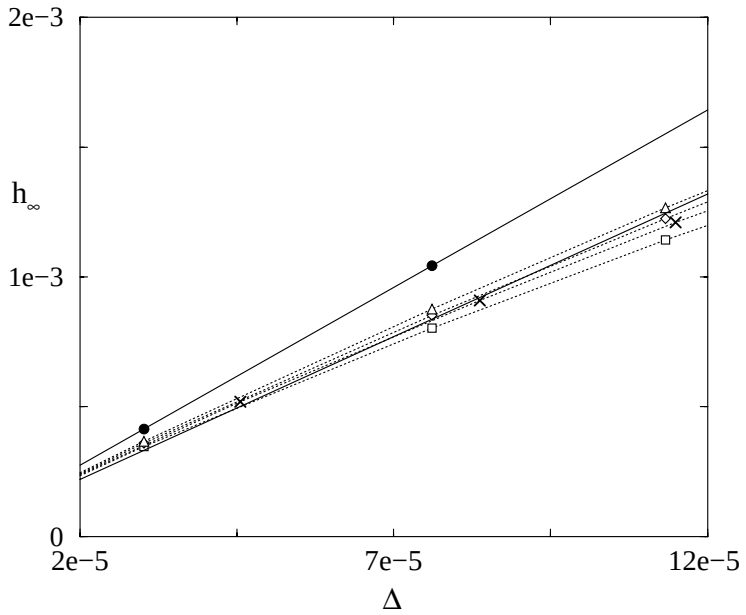


FIG. 3.1. *Comparison of $h_\infty$ for the solution of the full model* (2.3)–(2.5), (2.7)–(2.17)*, with the asymptotic prediction* (3.15) *(solid line with circles) and with the line determined in the experiments (solid line without symbols). Triangles, diamonds, and squares correspond to the numerical data points for $\alpha = 20^o$ and $\omega = 0.7$, 0.5, 0.3, respectively, and crosses are for $\alpha = 30^o$ and $\omega = 0.5$; dotted lines interpolate data points.*

Calculating higher corrections for the model (2.3)–(2.5), (2.7)–(2.17) in order to improve the accuracy of the asymptotic formula is a formidable task; the outer correction problems involves a full coupled system of Stokes and energy equations. However, from our numerical calculations we find that only the terms that are important either in the meniscus or in the film contribute significantly to the shape of the free surface. In the thin film, or lubrication regime, it suffices to retain only mass conservation (2.10), the boundary conditions for $u$, $w$ in (2.12) and (2.13), the $u_{zz}$ contribution to the viscosity, the dominant balance in the tangential stress condition ($u_z$ on the left- and $-T_x$ on the right-hand side of (2.14)), and to set the temperature to be constant in the $z$-direction, i.e., $T \equiv \Omega(x)$. For the normal stress condition, we retain only the pressure on the left and the curvature term on the right. We keep the full (not linearized) expression for the curvature, since it is needed in the meniscus region, in addition to both gravity terms.

The reduced model equations have the advantage that the bulk variables can be integrated out of the problem in the same manner as in the derivation of the usual lubrication equations. We obtain the following third order ODE for the shape $z = h(x)$ of the film:

$$h^3 \frac{d}{dx}\left(\frac{h_{xx}}{(1+h_x^2)^{3/2}}\right) = 3\delta(\Omega'(x)h^2 - h_\infty^2) - \cos\alpha(h^3 - h_\infty^3) + \sin\alpha h^3 h_x. \tag{3.16}$$

It is supplemented by (2.3) and by the boundary conditions (2.4), (2.5). Subsequently, we will refer to this model as the reduced (or simplified) model, and to the earlier

one, i.e., (2.3)–(2.5), (2.7)–(2.17), as the full model.

To see that $h_\infty$ is fixed in the reduced model, we first look at the asymptotic expansion for solutions $h$ of (3.16), (2.5) near $x \to \infty$, which is

$$h(x) \sim x \cot\alpha + d_1 + d_2 \exp((\sin\alpha)^{1/2} x) + d_3 \exp(-(\sin\alpha)^{1/2} x),$$

where $d_1$, $d_2$, and $d_3$ are constants. The boundary conditions (2.5) require $d_1 = -x_0 \cot\alpha$ and $d_2 = 0$. We need two more conditions to fix the solution of the third order ODE and $h_\infty$. If we linearize (3.16) near the flat state at $x \to -\infty$, by setting $h = h_\infty + \epsilon(x)$, $\epsilon(x) \ll h_\infty$, we obtain for $\epsilon(x)$ the equation

$$\epsilon_{xxx} = (6\delta h_\infty - 3h_\infty^2 \cos\alpha)\epsilon + h_\infty^3 \sin\alpha\, \epsilon_x.$$

This linear equation has exactly one mode that decays for $x \to -\infty$, provided that

$$2\delta - h_\infty \cos\alpha > 0. \tag{3.17}$$

In this case, two growing modes have to be excluded so that we get the two additional conditions we need. If (3.17) is not satisfied, we have two decaying modes, which eventually means that we have one condition less than necessary; $h_\infty$ is not uniquely determined. For the values of $h_\infty$ computed in this paper, (3.17) was always fulfilled.

To verify that all major contributions to the meniscus profile have been retained in (3.16), we solve the reduced model equations numerically, using essentially the same approach, regarding discretization and phase condition, as for the full model. Note that (3.16) can be written as (3.5) with $R(h) = h^{-3}[(3/2)(\Omega'(x)h^2 - h_\infty^2) + \delta^{-1}\cos\alpha\, h_\infty^3/2]$. The choice for $\Omega$ is the same as before (cf. (2.3)), as well as for the other parameters. In particular, we used the values for $\delta$ obtained for the adjusted temperature gradient. The lines in Figure 3.2 differ only slightly from their counterparts for the full model, and in consequence, agree nearly as well with the experimental line.

**4. Asymptotic approximations of the film thickness.** We seek a matched asymptotic solution for (3.16), (2.3)–(2.5), with the small parameter $\delta$. Furthermore, we restrict our attention to the range of $\alpha$ for which $\cos\alpha \sim 1$; this includes the range covered in the experimental survey [6], where $\alpha \le 30^o$.

Equations (3.16), (2.3)–(2.5) are stated in the outer variables. In the inner scaling, we expect the surface tension and the Marangoni term, which provides the driving force for the rising film, to enter the dominant balance. This leads to the new variables $h = \delta^{3\nu+1}\varphi$, $x = \delta^{2\nu+1/3}\xi$. There is still one unknown, $\nu$, in the inner scaling, which is natural since we need two balances to fix the scales. Unfortunately, there is no other obvious balance in (3.16) that could fix $\nu$, but from the experimental data [6] we know that the dimensional film thicknesses in the flat film are well below $\tau/\rho g$, i.e., that $h_\infty \ll \delta$. Note this is consistent with the asymptotic formula from [6] as given in (3.15).

From this it seems reasonable to seek the asymptotic solution for an inner scaling with $h \ll \delta$ or $\nu > 0$. Within this range, one finds that successful matching is possible only for $\nu = 1/3$. We will restrict our attention here to this case and set $\nu = 1/3$ in what follows. Then, we have $h = \delta^2\varphi$, $x = \delta\xi$, which yields the rescaled ODE

$$\varphi^3 \frac{d}{d\xi}\left(\frac{\varphi_{\xi\xi}}{(1+\delta^2\varphi_\xi^2)^{3/2}}\right) = 3(\Omega'(\delta\xi)\varphi^2 - h_\infty^2) - \delta\cos\alpha(\varphi^3 - h_\infty^3) + \delta^2 \sin\alpha \varphi^3 \varphi_\xi$$

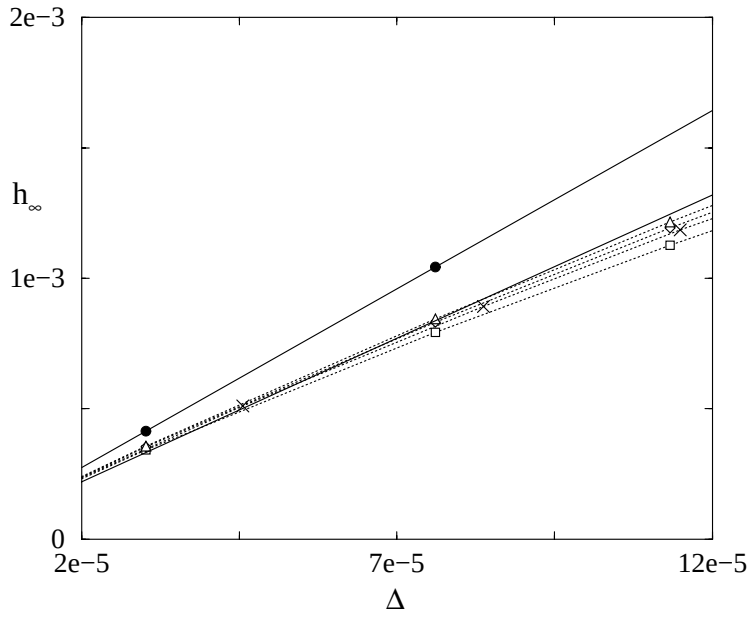


FIG. 3.2. *Comparison of $h_\infty$ for the solution of the reduced model* (3.16) *and* (2.3)–(2.5) *for $h_\infty$ with the asymptotic prediction* (3.15)*. Symbols carry over from Figure* 3.1*; note that the diamonds are partially covered by the triangles.*

and the boundary conditions

$$\lim_{\xi\to-\infty}\varphi = h_\infty/\delta^2, \quad \lim_{\xi\to-\infty}\varphi_\xi = 0, \quad \lim_{\xi\to-\infty}\varphi_{\xi\xi} = 0.$$

The equations for $h$ and $\varphi$ together with the boundary conditions for $\varphi$ suggest the following asymptotic expansions:

$$\begin{aligned} h &= h_0 + \delta h_1 + \cdots, \\ \varphi &= \varphi_0 + \delta\varphi_1 + \cdots, \\ h_\infty &= \delta^2\varphi_{\infty,0} + \delta^3\varphi_{\infty,1} + \cdots. \end{aligned}$$

This yields the following leading order, outer, and inner problems, respectively:

$$\frac{d}{dx}\left(\frac{h_{0xx}}{(1+h_{0x}^2)^{3/2}}\right) = -\cos\alpha + \sin\alpha\, h_{0x}, \tag{4.1}$$

$$\lim_{x\to\infty}(h_0 - (x-x_0)\cot\alpha) = 0, \quad \lim_{x\to\infty} h_{0xx} = 0, \tag{4.2}$$

and

$$\begin{aligned} &\varphi_0^3\varphi_{0\xi\xi\xi} = 3(\varphi_0^2 - \varphi_{\infty,0}^2), \\ &\lim_{\xi\to-\infty}\varphi_0 = \varphi_{\infty,0}, \quad \lim_{\xi\to-\infty}\varphi_{0\xi} = 0, \quad \lim_{\xi\to-\infty}\varphi_{0\xi\xi} = 0. \end{aligned}$$

The latter problem can be scaled into a parameter-free form, however, by introducing the new variables $\varphi = \varphi_{\infty,0}\phi_0$ and $\xi = \varphi_{\infty,0}^{2/3}(\eta + \hat\eta)$, yielding

$$\phi_0^3\phi_{0\eta\eta\eta} = 3(\phi_0^2 - 1), \tag{4.3}$$

$$\lim_{\eta\to-\infty}\phi_0 = 1, \quad \lim_{\eta\to-\infty}\phi_{0\eta} = 0, \quad \lim_{\eta\to-\infty}\phi_{0\eta\eta} = 0. \tag{4.4}$$

The shift $\hat{\eta}$ has been included in the rescaling so that we can later fix a specific $\phi_0$; note that both the original and the rescaled inner problems are autonomous and therefore translationally invariant.

On linearizing the equation around the flat state $\phi_0 = 1 + \Phi$, with $|\Phi| \ll 1$, we find that there is only one mode that decays for $\eta \to -\infty$; the others grow exponentially in this limit and therefore have to be excluded. The remaining mode, $\Phi = \text{const}\exp(6^{1/3}\eta)$, leads to a solution $\phi_0$ of the nonlinear problem that decays to zero in finite time, if const $< 0$, thus becoming singular; it is evidently not the solution we need.

If const $> 0$, we get a solution that grows unboundedly. This can be seen by noting that in this case, all derivatives of $\phi_0$ are positive and monotone increasing. For this solution, we find the following expansion at $\eta \to \infty$:

$$\phi_0 = a\eta^2 - \frac{3}{a}\eta \ln \eta + o(\eta).$$

Here we have made use of the translational invariance of (4.3) and (4.4) to eliminate the linear term, thereby selecting a specific $\phi_0$ from the one-parameter family of solutions. The coefficient $a$ of the leading term has to be determined numerically, with the result that $a = 1.89411$.

Transforming this solution back into the original inner variables $\xi$ and $\varphi$, we obtain the following expansion at $\xi \to \infty$:

$$\varphi_0(\xi) = \varphi_{\infty,0}\phi_0(\xi\varphi_{\infty,0}^{-2/3} - \hat{\eta}) = a\varphi_{\infty,0}^{-1/3}\xi^2 + o(\xi^2),$$

which in outer scales reads as

$$\delta^2\varphi_0 = a\varphi_{\infty,0}^{-1/3}x^2 + \cdots. \tag{4.5}$$

The expansion for the outer solution is simply given by the Taylor expansion at $x = 0$,

$$h_0 = h_0(0) + h_{0x}(0)x + Ax^2 + o(x^3).$$

Comparing this to (4.5) we obtain the matching condition

$$h_0(0) = 0, \qquad h_{0x}(0) = 0, \qquad A = a\varphi_{\infty,0}^{-1/3}. \tag{4.6}$$

The first two conditions and (4.1), (4.2) are precisely the equations for the static meniscus, which are solved in the appendix. From the calculations there, we get

$$A = \left(\frac{1 - \sin\alpha}{2}\right)^{1/2},$$

and from the third matching condition

$$\varphi_{\infty,0} = \left(\frac{2a^2}{1 - \sin\alpha}\right)^{3/2},$$

and for $h_\infty$, to leading order in $\delta$,

$$h_\infty = 2a^3\left[\frac{\delta^2}{2}\left(\frac{2}{1 - \sin\alpha}\right)^{3/2}\right] = 13.591\Delta.$$

Thus, we recover the leading order formula of [4, 6], except for a small deviation in the constant, possibly due to a slight difference in the numerical accuracy.

We now proceed to calculating the next order correction for $h_\infty$. We get the outer problem

$$\frac{d^2}{dx^2}\left(\frac{h_{1x}}{(1+h_{0x}^2)^{3/2}}\right) = \frac{3\Omega'(x)}{h_0} + \sin\alpha\; h_{1x},$$
$$\lim_{x\to\infty} h_1 = 0, \quad \lim_{x\to\infty} h_{1x} = 0 \tag{4.7}$$

and the inner problem

$$\varphi_0^3\varphi_{1\xi\xi\xi} = -3\varphi_0\varphi_1 + 9\frac{\varphi_1}{\varphi_0}\varphi_{\infty,0}^2 - 6\varphi_{\infty,0}\varphi_{\infty,1} - \cos\alpha\left(\varphi_0^3 - \varphi_{\infty,0}^3\right),$$
$$\lim_{\xi\to-\infty}\varphi_1 = \varphi_{\infty,1}, \qquad \lim_{\xi\to-\infty}\varphi_{1\xi} = 0, \quad \lim_{\xi\to-\infty}\varphi_{1\xi\xi} = 0.$$

For the outer problem, an expression for the solution can be written down quite easily, starting from the observation that we are really dealing with a second order ODE for $h_{1x}$ for which one solution of the homogeneous problem is easily found to be $h_{0xx}$. One gets

$$h_1 = D_0 + D_1 h_{0x} + D_2\int_{\omega x_0}^{x}\frac{(1+h_{0x}^2)^3}{h_{0xx}^2}ds + p(x;\omega,\alpha), \tag{4.8}$$

where

$$p(x;\omega,\alpha) = \int_0^x h_{0xx}\int_{\omega x_0}^{t}\frac{(1+h_{0x}^2)^3}{h_{0xx}^2}\int_{\omega x_0}^{s}\frac{3\Omega' h_{0xx}}{h_0(1+h_{0x}^2)^{3/2}}dr\,ds\,dt.$$

The symbols $D_0$, $D_1$, and $D_2$ denote constants of integration. Since the first terms and the last term in (4.8) are bounded as $x\to\infty$—in fact, $p(x) = p(\omega x_0)$ for $x \geq \omega x_0$—but the third is not, it follows from (4.7) that $D_2 = 0$, and furthermore

$$D_0 + D_1\cot\alpha + p(\omega x_0;\omega,\alpha) = 0. \tag{4.9}$$

Via the integral representation for $p$ we easily find the expansion

$$p = p_1 x - \frac{3}{A}x\ln x + p_2 x^2 + \frac{\cos\alpha}{4A^2}x^2\ln x + O(x^3),$$

where $p_1 = p_1(\omega,\alpha)$ and $p_2 = p_2(\omega,\alpha)$ had to be obtained numerically for each $\omega$ and $\alpha$. This yields for $h_1$

$$h_1 = D_0 + (p_1 + 2AD_1)\;x - \frac{3}{A}x\ln x + \left(p_2 - \frac{D_1\cos\alpha}{2}\right)x^2 + \frac{\cos\alpha}{4A^2}x^2\ln x + O(x^3).$$

As before, the numerical work required for the inner problem can be reduced by rescaling the equation so that $\varphi_1(\xi) = \varphi_{\infty,1}\phi_1(\eta)$; the independent variable and $\varphi_0$ are rescaled as before. We get

$$\phi_{1\eta\eta\eta} = \left(-\frac{3}{\phi_0^2} + \frac{9}{\phi_0^4}\right)\phi_1 - \frac{6}{\phi_0^3} + \frac{\varphi_{\infty,0}^2\cos\alpha}{\varphi_{\infty,1}}\left(\frac{1}{\phi_0^3} - 1\right), \tag{4.10}$$

$$\lim_{\eta\to-\infty}\phi_1 = 1, \quad \lim_{\eta\to-\infty}\phi_{1\eta} = 0, \quad \lim_{\eta\to-\infty}\phi_{1\eta\eta} = 0. \tag{4.11}$$

We quickly find that $\phi_{0\eta}$ is a solution of the homogeneous solution, and, in fact, is the only solution (up to an arbitrary constant) which decays at $-\infty$. The other two modes grow exponentially and, thus, have to be excluded. The general solution of (4.10) that is consistent with (4.11) can therefore be written as

$$\phi_1 = \text{const}\ \phi_{0\eta} + \phi_0 - \frac{2}{3}\eta\phi_{0\eta} + \frac{\varphi_{\infty,0}^2 \cos\alpha}{\varphi_{\infty,1}} F, \tag{4.12}$$

where $F$ is any special solution of

$$F_{\eta\eta\eta} = \left(-\frac{3}{\phi_0^2} + \frac{9}{\phi_0^4}\right) F + \left(\frac{1}{\phi_0^3} - 1\right)$$

with homogeneous boundary conditions.

We can expand (4.12) at $\eta \to \infty$ to the order needed later for the matching:

$$\phi_1 = \frac{\varphi_{\infty,0}^2 \cos\alpha}{\varphi_{\infty,1}} \left(-\frac{\eta^3}{6} + \frac{\eta^2}{4a^2}\ln\eta + c_1\eta^2\right) + c_2\eta^2 + O(\eta\ln\eta),$$

where $c_1$ and $c_2$ are constants that do not depend on $\alpha$ (nor on $\omega$); the first has to be determined numerically; the second comes from the expansion for $\phi_0 - 2\eta\phi_{0\eta}/3$. We found $c_1 = -0.151$, $c_2 = -a/3 = -0.63137$. We remark that since $\phi_{0\eta} = O(\eta)$, the contribution from the homogeneous solution does not affect the expansion to the order given here. Therefore, the solution of the inner correction problem will be determined only up to an arbitrary contribution of $\varphi_{0\xi}$, in a similar way as $\hat\eta$ is not fixed by the leading order matching.

We now have all the information necessary to write down the expansion for $h_0 + \delta h_1$ and $\delta^2\varphi_0 + \delta^3\varphi_1$ in outer variables:

$$\begin{aligned} h_0 + \delta h_1 = {} & Ax^2 - \frac{\cos\alpha}{6}x^3 + \cdots + D_0\delta - \frac{3}{A}\delta x\ln x + (p_1 + 2AD_1)\,\delta x \\ & + \frac{\cos\alpha}{4A^2}\delta x^2\ln x + \left(p_2 - \frac{D_1\cos\alpha}{2}\right)\delta x^2 + \cdots, \\ \delta^2\varphi_0 + \delta^3\varphi_1 = {} & Ax^2 - \frac{3}{A}\delta x\ln(x/\delta) + \left(\frac{3}{A}\ln\varphi_{\infty,0}^{2/3} - \frac{2a^2}{A}\hat\eta\right)\delta x + \cdots \\ & - \frac{\cos\alpha}{6}x^3 + \frac{\cos\alpha}{4A^2}\delta x^2\ln(x/\delta) + \left[\frac{2a^2\cos\alpha}{1-\sin\alpha}\left(c_1 + \frac{\hat\eta}{2}\right)\right. \\ & \left. - \frac{\cos\alpha}{4A^2}\ln\varphi_{\infty,0}^{2/3} + c_2\frac{(1-\sin\alpha)^2}{4a^4}\varphi_{\infty,1}\right]\delta x^2. \end{aligned}$$

One observes that the logarithmic terms can be matched only if, in the expansion of the inner solution, $\ln(x/\delta)$ is split and the $\ln\delta$ contributions are grouped with the terms that are pure integer powers in $x$. This leads to the appearance of *logarithmic switchback* terms in $\delta$ in the matching conditions, in the solution for

$$\begin{aligned} \varphi_{\infty,1} = {} & \frac{a^4\cos\alpha}{4A^5c_2}\,p_1(\omega,\alpha) + \frac{a^4}{A^4c_2}\,p_2(\omega,\alpha) - \frac{a^4\cos\alpha}{2A^6c_2}\ln\left(\delta\varphi_{\infty,0}^{2/3}\right) \\ & - \frac{a^6c_1\cos\alpha}{A^6c_2}, \end{aligned}$$

and also in the shift

$$\hat\eta = \frac{3}{2a^2}\ln\left(\delta\varphi_{\infty,0}^{2/3}\right) - \frac{A}{2a^2}\,p_1(\omega,\alpha) + \frac{A^2}{a^2\cot\alpha}\,p(\omega x_0;\omega,\alpha).$$

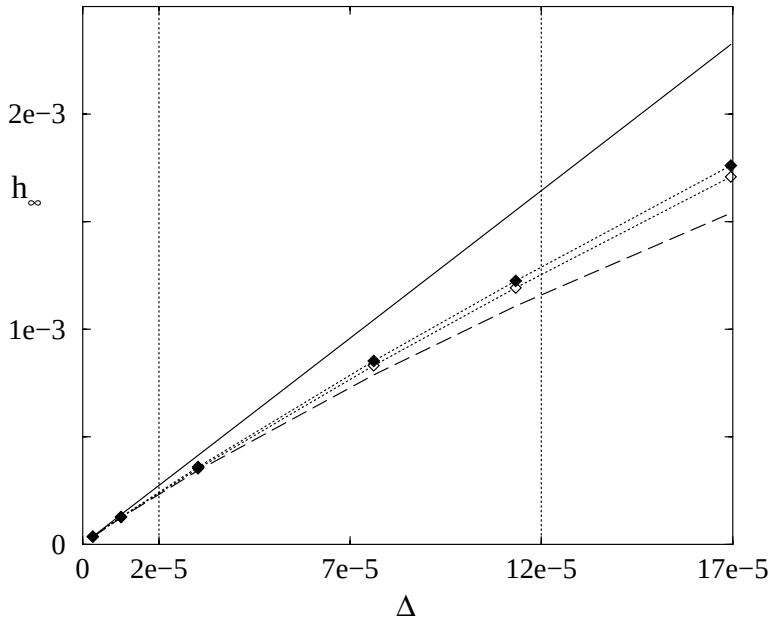


FIG. 4.1. *Comparison of $h_\infty$ for the solution of the reduced model (open diamonds interpolated by a dotted line) with the asymptotic prediction to leading and to next order (solid and dashed line, respectively). The parameters are $\alpha = 20^\circ$ and $\omega = 0.5$. The filled diamonds, interpolated by a dotted line, denote the results for the full model. The dotted vertical lines delimit the range of $\Delta$ covered in the experiments in* [6].

We refer to, e.g., [11] for background information on logarithmic switchback terms in matched asymptotic expansions. The matching conditions also yield $D_0 = 0$, and from this and (4.9) we get $D_1 = -p(\omega x_0; \omega, \alpha)/\cot\alpha$.

In Figure 4.1 the asymptotic approximations are compared with the numerical results for the reduced and for the full model by plotting all four values for $h_\infty$ versus $\Delta$, with $\Delta$ defined as before (cf. (3.15)). The parameters $\alpha = 20^\circ$ and $\omega = 0.5$ are held fixed. For small $\Delta < 2 \cdot 10^{-5}$ (correspondingly, small $\delta$), the agreement even between the leading order and the numerical value for the reduced model is acceptable, but it deteriorates rapidly once we reach the range of $\Delta$ covered by the experiments in [6], as we observed before. The next order correction substantially improves the agreement in this range.

**5. Further questions.** So far, we have concentrated on the small-$\alpha$-regime, $\alpha \leq 30^\circ$; in particular, our derivation of the asymptotic solution required $\cos\alpha \sim 1$. If we increase $\alpha$ while keeping $\delta$ fixed, the values calculated with the leading order asymptotic formula differ dramatically from the numerical results—for both the full and the reduced model. This signals a breakdown of our asymptotic solution and the transition to a different scaling regime. In an upcoming paper [16], we therefore return to the reduced model and investigate what happens for moderate and large $\alpha$. At this point, we restrict ourselves to a preliminary result which takes up an observation by Wilson [21] for the drag-out problem.

As we increase $\alpha$, we find that $h_\infty$ increases faster than the threshold $2\delta/\cos\alpha$ imposed by (3.17); recall that this condition has to be fulfilled in order for the solution

for $h_\infty$ to be (locally) unique. In fact, for $\omega$ somewhat larger than those discussed in this paper, our numerical calculations indicate that there is a value $\alpha_c < 90^o$ for which $2\delta - h_\infty \cos\alpha \to 0$ as $\alpha \uparrow \alpha_c$. In the limiting case with no cut-off (i.e., $\omega = \infty$), for example, we get $\alpha_c \approx 78^o \ldots 87^o$ for $\delta$ in the range of $0.01 \ldots 0.001$. For $\alpha > \alpha_c$, there appears to be no solution for $h_\infty$ which satisfies the condition (3.17). This situation seems to persist if we decrease $\omega$ to values of $\omega \approx 3$, with typically an increase in $\alpha_c$ for smaller $\omega$. This tendency is consistent with the observation that cutting off the shear stress earlier tends to produce thinner films; see also Figure 3.2.

For the choices of $\omega < 1$ typically used in this paper and $\delta = 3.375 \cdot 10^{-3}$, the film height remains below the threshold imposed by (3.17), at least for those angles for which the film shape could be computed. Our numerical codes fail to converge to a solution for $h$ and $h_\infty$ for $\alpha$ around $80^o$, possibly indicating that a different type of transition might take place, e.g., that the shear stress might not be sufficient to maintain a thin film for these cut-off positions and inclination angles.

Experimentally, [19] observe that for large $\alpha$, there is indeed a transition in the film formation, because the rear part of the double wave structure that prevails near the contact-line in this $\alpha$-regime no longer separates from the meniscus. However, the transition occurs at $\alpha \approx 70^o$, well below the aforementioned inclination angles. In [16], we will return to this question and discuss how the properties of our reduced model fit in with recent results [2, 3, 17] on the wave structure near the contact-line.

**Appendix. The static meniscus.** In this appendix, we derive some results on the static meniscus, that is, when no Marangoni shear stress, and hence no flow, is present. These calculations yield an expression for the distance $x_0$ the meniscus rises with respect to the level of the reservoir, and they are also needed for the leading order outer solution in section 4. For general information on the shape of static menisci, we refer the reader to the standard literature on fluid mechanics, e.g., [13]. Most of the derivations below can also be found in [21].

The shape $z = h(x)$ of the static meniscus is governed by the balance of the pressure contribution from gravity, $(p_x, p_z) = (\rho g \cos\alpha, -\rho g \sin\alpha)$, and surface tension, $p = -\sigma h_{xx}(1 + h_x^2)^{-3/2}$. After eliminating the pressure and nondimensionalizing with the capillary length $L$, one obtains the ODE (4.1).

The boundary conditions at $x \to \infty$ are obtained from the requirement that the meniscus levels out onto the surface of the reservoir, i.e., $h$ must satisfy (4.2). For the boundary conditions at $x \to -\infty$, we use $h(0) = h_x(0) = 0$. They arise in the context of the derivation of the matched asymptotic expansion as part of the leading order matching conditions (4.6) and for the static meniscus, because silicon oil completely wets the silicon wafer (zero contact angle).

We can integrate this equation once,

$$\frac{d}{dx}\left(\frac{h_x}{(1+h_x^2)^{1/2}}\right) = -(x - x_0)\cos\alpha + h\sin\alpha. \tag{A.1}$$

Here the constant of integration has been fixed by using the boundary conditions (4.2). We integrate this equation once more, again using (4.2) to deal with the constant of integration. The result is

$$\frac{h_x \cos\alpha + \sin\alpha}{(1+h_x^2)^{1/2}} = 1 - \frac{1}{2}\left(-(x - x_0)\cos\alpha + h\sin\alpha\right)^2. \tag{A.2}$$

Evaluating (A.2) at $x = 0$ and exploiting the boundary conditions at this point yields an equation for $x_0$ for which we compute the positive solution to be

$$x_0 = \frac{(2 - 2\sin\alpha)^{1/2}}{\cos\alpha}.$$

Inserting $x_0$ and again the boundary conditions at $x = 0$ into (A.1) yields

$$h_{xx}(0) = (2 - 2\sin\alpha)^{1/2}.$$

**Acknowledgments.** The author would like to thank Dr. B. Wagner for many stimulating discussions and critical comments during the preparation of this work. He also thanks Prof. T. Witelski, Prof. A. Bertozzi, and Prof. M. Shearer for their help on several questions. The author is also indebted to Prof. Brokate and Prof. Hoffmann for creating a supportive research environment.

**Note added in proof.** While this article was under review, an article by L. Schwartz [20] appeared, where the author came up with a model similar to our reduced model for the case $\alpha = 0$. Here, we validate our reduced model by numerical comparison with the corresponding full Stokes problem. Our asymptotic analysis differs to next order in that, for the purpose of matching, we split the $\ln\xi$ terms in the inner expansion into $\ln x - \ln\delta$. The second of these terms appears as logarithmic switchback of $O(\delta^3 \ln\delta)$ in the correction for the film thickness, together with a contribution $O(\delta^3)$.

## REFERENCES

[1] E. Anderson, Z. Bai, C. Bischof, J. Demmel, J. Dongarra, J. Du Croz, A. Greenbaum, S. Hammarling, A. McKenney, S. Ostrouchov, and D. Sorenson, *LAPACK Users' Guide*, 2nd ed., SIAM, Philadelphia, 1995.

[2] A. L. Bertozzi, A. Münch, X. Fanton, and A. M. Cazabat, *Contact line stability and 'undercompressive shocks' in driven thin film flow*, Phys. Rev. Lett., 81 (1998), pp. 5169–5172.

[3] A. L. Bertozzi, A. Münch, and M. Shearer, *Undercompressive waves in driven thin film flow*, Phys. D, 134 (1999), pp. 431–464.

[4] P. Carles and A.-M. Cazabat, *The thickness of surface-tension-gradient-driven spreading films*, J. Colloid and Interface Science, 157 (1993), pp. 196–201.

[5] A. M. Cazabat, F. Heslot, S. M. Troian, and P. Carles, *Finger instability of thin spreading films driven by temperature gradients*, Nature, 346 (1990), pp. 824–826.

[6] X. Fanton, A. M. Cazabat, and D. Quéré, *Thickness and shape of films driven by a Marangoni flow*, Langmuir, 12 (1996), pp. 5875–5880.

[7] M. J. Friedman and E. J. Doedel, *Numerical computation and continuation of invariant manifolds connecting fixed points*, SIAM J. Numer. Anal., 28 (1991), pp. 789–808.

[8] E. B. Hansen, *Stokes flow down a wall into an infinite pool*, J. Fluid Mech., 178 (1987), pp. 243–256.

[9] D. E. Kataoka and S. M. Troian, *A theoretical study of instabilities at the advancing front of thermally driven coating films*, J. Colloid and Interface Science, 192 (1997), pp. 350–362.

[10] D. E. Kataoka and S. M. Troian, *Stabilizing the advancing front of thermally driven climbing films*, J. Colloid and Interface Science, 203 (1998), pp. 335–344.

[11] P. A. Lagerstrom and R. G. Casten, *Basic concepts underlying singular perturbation techniques*, SIAM Rev., 14 (1972), pp. 63–120.

[12] L. Landau and B. Levich, *Dragging of a liquid by a moving plate*, Acta Physicochim. URSS, 17 (1942), pp. 42–54.

[13] L. D. Landau and L. D. Lifshitz, *Fluid Mechanics*, 2nd ed., Pergamon Press, Oxford, 1989.

[14] V. Ludviksson and E. N. Lightfoot, *The dynamics of thin liquid films in the presence of surface-tension gradients*, Am. Inst. Chem. Engrs. J., 17 (1971), pp. 1166–1173.

[15] H. K. Moffatt, *Viscous and resistive eddies near a sharp corner*, J. Fluid Mech., 18 (1964), pp. 1–18.

[16] A. Münch, *Spreading of Thin Marangoni-Driven Films at Capillary Menisci*, manuscript.
[17] A. Münch, *Shock transitions in Marangoni-gravity driven thin film flow*, Nonlinearity, 13 (2000), pp. 731–746.
[18] A. Münch and A. L. Bertozzi, *Rarefaction-undercompressive fronts in driven films*, Phys. Fluids, 11 (1999), pp. 2812–2814.
[19] M. Schneemilch and A. M. Cazabat, *Shock separations in wetting films driven by thermal gradients*, Langmuir, 16 (2000), pp. 9850–9856.
[20] L. W. Schwartz, *On the asymptotic analysis of surface-stress-driven thin-layer flow*, J. Engrg. Math., 39 (2001), pp. 171–188.
[21] S. D. R. Wilson, *The drag-out problem in film coating theory*, J. Engrg. Math., 16 (1982), pp. 209–221.